Progress in Reaction Kinetics and Mechanism

ARTICLE

Open Access

https://doi.org/10.48130/prkm-0025-0028

Progress in Reaction Kinetics and Mechanism **2026**, 51: e001

Ab initio kinetic study of decomposition reactions of the unsym-dimethylhydrazine radical $HNN(CH_3)_2$

Wei Li[#*], Yi Zhang[#], Qilong Fang[*], Jun Fang and Yuyang Li

School of Mechanical Engineering, Shanghai Jiao Tong University, Shanghai 200240, China

[#] Authors contributed equally: Wei Li, Yi Zhang

[*] Correspondence: lw2017@sjtu.edu.cn (Li W); fangqilong@sjtu.edu.cn (Fang Q)

Abstract

Unsym-dimethylhydrazine (UDMH) is an important nitrogen-containing liquid propellant fuel commonly combined with nitrogen tetroxide (NTO) in hypergolic systems. In this work, theoretical calculations were performed on the decomposition reactions of critical UDMH radical, $HNN(CH_3)_2$ to get insight into its combustion chemical kinetics. Specifically, reactions of its isomerization, β-scission, and H-abstraction reactions attacked by NO_2 and NO, as well as the subsequent decomposition reactions of formed $NN(CH_3)_2$ were investigated. Potential energy surfaces (PESs) for these reactions were obtained by employing the CCSD(T)/CBS(D+T)//M06-2X/def2-TZVP method. The RRKM/Master Equation approach was used to calculate the temperature- and pressure-dependent rate constants. Comparisons with monomethylhydrazine (MMH) radicals were made to elucidate the effect of CH_3-group substitution on the kinetic characteristics of UDMH-radical decomposition. For isomerization and β-scission reactions of $HNN(CH_3)_2$, it undergoes β-N-C scission reaction more readily than H-migration isomerization to $H_2NN(CH_3)CH_2$. Additionally, the rate constants for β-scission reactions of UDMH radicals are close to those of MMH radicals. For the H-abstraction reactions of $HNN(CH_3)_2$ by NO_2, the reaction forming $NN(CH_3)_2$ and *cis*-HONO from the decomposition of *cis*-$ONON(H)N(CH_3)_2$ has the highest rate constants, which differ significantly from the H-abstraction of MMH radical ($HNN[H]CH_3$). $HNN(CH_3)_2$ primarily undergoes H-abstraction at the terminal nitrogen site, forming $NN(CH_3)_2$, whereas $HNN(H)CH_3$ prefers H-abstraction from the central nitrogen atom. The H-abstraction reaction of $HNN(CH_3)_2$ by NO also easily produces $NN(CH_3)_2$. Subsequently, $NN(CH_3)_2$ dissociates via a low-barrier pathway to produce N_2 and C_2H_6. The calculated rate constants provide important parameters for the kinetic modeling development of UDMH/NTO combustion.

Citation: Li W, Zhang Y, Fang Q, Fang J, Li Y. 2026. *Ab initio* kinetic study of decomposition reactions of the unsym-dimethylhydrazine radical $HNN(CH_3)_2$. *Progress in Reaction Kinetics and Mechanism* 51: e001 https://doi.org/10.48130/prkm-0025-0028

Introduction

The combination of unsym-dimethylhydrazine (UDMH) and nitrogen tetroxide (NTO) is a widely adopted hypergolic bipropellant in liquid rocket propulsion systems, including spacecraft (e.g., launch vehicles and satellite propulsion systems) and missile technology[1]. This mixture ignites spontaneously upon contact, requiring no ignition system. This unique combustion behavior makes the study of its fundamental combustion characteristics particularly critical. However, the high toxicity and corrosiveness of UDMH strongly hinder the related experimental investigations on its combustion characteristics. Although some kinetic models for hydrazine-based fuel/NTO systems have been developed and analyzed[2–6] on the basis of previous theoretical calculations, the accuracy of the rate constants of elementary reactions still requires further refinement. Under this background, high-performance theoretical calculations using a quantum chemical method provide a safer alternative for understanding the chemical structure and the corresponding elementary reactions, which is of critical importance for understanding combustion characteristics and developing kinetic model.

To date, theoretical studies on hydrazine-based fuel/NTO bipropellant systems have primarily focused on thermal decomposition and H-abstraction reactions. Sun et al.[7,8] conducted systematic theoretical investigations on methylhydrazine (MMH), examining both thermal decomposition and H-abstraction pathways. Their results demonstrated that H-abstraction from the terminal amine site, where it forms the *trans*-$HNN(H)CH_3$ radical, represents the predominant reaction channel among various possible abstraction routes. Tang et al.[9] employed BMC-CCSD//B3LYP/6-311G(d,p) level of theory to calculate rate constants for H-abstraction reactions between UDMH and OH. Wang et al.[10] and Kanno et al.[11] independently investigated H-abstraction reactions involving the H atom, utilizing different theoretical approaches. Specifically, Wang et al.[10] applied canonical variational transition state theory with small-curvature tunnelling correction (CVT/SCT) at the MCG3MPWPW91//MPW1K/6-311G(d,p) level, whereas Kanno et al.[11] employed CBS-QB3//DSD-BLYP-D3(BJ)/def2-TZVP in combination with transition state theory (TST), respectively. These investigations consistently revealed that, similar to MMH, H-abstraction from the terminal amine site of UDMH is thermodynamically favored over abstraction from the methyl site.

Regarding the successive decomposition reactions of fuel radicals, Kanno et al.[12] conducted computational studies on the reactions of NO_2 with three MMH-derived radicals ($HNN(H)CH_3$, H_2NNCH_3, and $H_2NN(H)CH_2$), using quantum chemical calculations and steady-state unimolecular master equation (ME) analysis based on Rice-Ramsperger-Kassel-Marcus (RRKM) theory. Their work yielded temperature- and pressure-dependent, product-specific rate coefficients for these reactions. The results demonstrated that the reactivity of these radicals with NO_2 depends strongly on both the heights of the roaming transition-state barriers between RNO_2 and RONO and the energy barriers for dissociation pathways. More recently, Bai et al.[13] extended this investigation to examine not only the initial H-abstraction reactions but also the subsequent H-abstraction processes involving NO_2 and the primary radical product ($HNNCH_3$). Computational methods, including the CCSD(T)/CBS//M06-2X/6-311++G(d,p) single-reference approach and the MRCI(7e,6o)/CBS//M06-2X/6-311++G(d,p) multi-reference method,

were adopted. Using the RRKM/ME approach, they obtained temperature- and pressure-dependent rate constants. These investigations revealed that these reactions play a crucial role in enhancing the overall combustion reactivity of the MMH/NO_2 system. It can be concluded that the successive decomposition reactions of fuel radicals in hydrazine-based fuels are of critical importance. However, existing theoretical calculations have primarily focused on MMH-derived radicals, with comparatively little research attention devoted to UDMH-derived radicals, despite UDMH's superior propellant characteristics, including its higher energy density. Furthermore, current studies have largely neglected other crucial decomposition pathways of these fuel radicals, such as isomerization reactions and β-scission reactions, which represent important decomposition mechanisms.

Prior computational studies[14] have demonstrated that although H-abstraction reactions can generate two distinct fuel radicals, $HNN(CH_3)_2$ and $H_2NN(CH_3)CH_2$, the former represents the fuel-specific N-involved radical and is more preferentially formed. Consequently, this work systematically examines the decomposition pathways of $HNN(CH_3)_2$, including isomerization processes, β-scission reactions, and H-abstraction reactions with NO_2 and NO oxidizers. The study employs high-level quantum chemical methods to characterize the complete potential energy surfaces and obtain temperature-dependent rate constants for these elementary reactions. A comprehensive comparative analysis is subsequently conducted to elucidate the dominant reaction mechanisms and their relative importance across different temperature regimes, with particular emphasis on the similarities and differences relative to MMH.

Theoretical methods

In this paper, the structure optimizations and frequency calculations for UDMH and its products were performed using the M06-2X method[15] combined with the def2-TZVP[16] basis set. The zero-point energy correction factor is 0.971[17], and the frequency correction factor is 0.984[17]. The intrinsic reaction coordinate (IRC) approach was utilized to ensure the accuracy of the transition state structures and to derive the corresponding reactant and product geometries. The low-frequency torsional modes with wave numbers below 300 cm^{-1} were identified as potential hindered rotors. For each identified torsional mode, a relaxed potential energy surface (PES) scan was performed by varying the corresponding dihedral angle in steps of 10° over a 360° range. All other geometric parameters were optimized at the M06-2X/def2-TZVP level of theory. Detailed results of electronic structure calculations are provided in the Supplementary File 1.

For high-precision single-point energy (SPE) calculations of stable molecules and transition states, coupled cluster methods combined with the cc-pVDZ and cc-pVTZ basis sets were used to obtain the energies, which were then extrapolated to the complete basis set energies using Eq. (1)[18]. In the previous theoretical work on the unimolecular decomposition and H-abstraction reaction of UDMH[14], the convergence of this level of theory was evaluated using larger basis sets (cc-pVQZ and cc-pVTZ). It was found that the calculated SPEs for the UDMH decomposition reactions at the CCSD(T)/CBS(T+Q) level were within 1 kcal/mol of those obtained at the CCSD(T)/CBS(D+T) level, indicating the feasibility of the originally chosen theoretical approach. As reported by Lee & Taylor[19], T1 diagnostic values were defined as the Frobenius norm of the single substitution amplitudes vector of the closed-shell CCSD wave function divided by the square root of the number of correlated electrons to address size consistency, and the recommended upper limits of T1 diagnostic values are ≤ 0.025 for reactant species, ≤ 0.035 for product radicals, and ≤ 0.044 for transition states. As shown in Supplementary Table S1, all T1 diagnostic values in this study met these requirements, which demonstrates that the single-reference method can reliably describe the wave function. All quantum chemical calculations for geometry optimization, frequency analysis, and rotational potential scans were performed using the Gaussian 09 program[20].

$$E_{\mathrm{CCSD(T)/CBS(D+T)}} = E_{\mathrm{CCSD(T)/cc-pVTZ}} + (E_{\mathrm{CCSD(T)/cc-pVTZ}} - E_{\mathrm{CCSD(T)/cc-pVDZ}}) \times 3^4/(4^4-3^4) \quad (1)$$

For the calculation of rate constants of reactions with tight transition state, such as the isomerization and β-scission reactions of $HNN(CH_3)_2$ radical, rate constants were determined using transition state theory (TST) based on the PES results. For the barrierless reactions of $HNN(CH_3)_2$ with NO_2 and NO, variational transition state theory (VTST) combined with the multi-reference method was applied. The CASPT2[21] method with the cc-pVDZ basis set was used to calculate the minimum energy paths (MEPs) for the corresponding N-N bond dissociation processes in their products. An active space of (6e,5o) was selected[22]. Based on the optimized geometries at CASPT2, the multi-reference configuration interaction method (MRCI) with the cc-pVDZ and cc-pVTZ basis sets is used to calculate higher-level single point energies, which are extrapolated to the CBS level using Eq. (2)[23]:

$$E_{\mathrm{MRCI(6e,5o)/CBS}} = E_{\mathrm{MRCI(6e,5o)/cc-pVTZ}} + (E_{\mathrm{MRCI(6e,5o)/cc-pVTZ}} - E_{\mathrm{MRCI(6e,5o)/cc-pVDZ}}) \times 2^3/(3^3-2^3) \quad (2)$$

Zero-point energy (ZPE) correction is included in the final energy of the optimized structures. Notably, the formation of pre- and post-reaction van der Waals complexes (i.e., reactant and product complexes) can influence reaction barriers and quantum tunneling effects. Therefore, it is common practice to account for them in rate constant calculations. In this work, phase space theory[24] was utilized to estimate the microcanonical rate constants, where the potentials along the reaction coordinate were estimated by $V = 10/R^6$, and the factor ten has the dimension of $Bohr^6$[25]. The RRKM theory combined with the ME method[26] was employed to compute the pressure-dependent rate constants. The partition functions of reactants and transition states were approximated using the rigid rotor harmonic oscillator (RRHO) model. The low-frequency torsional mode treated as a one-dimensional (1D) hindered rotor[27]. During rate constant calculation, the partition function of the identified hindered rotor mode replaced the original harmonic oscillator partition function and was subsequently used in the transition state theory calculations to obtain more accurate thermodynamic data and rate constants. Tunneling effects were accounted for using the 1D asymmetric Eckart model[28] in the rate constant calculations. The collisional energy transfer model was treated using the empirical formula: $\langle\Delta E\rangle_{\mathrm{down}} = 200(T/300)^{0.85}$[13]. The Lennard-Jones parameters σ = 5.65 Å and ε = 258.55 cm^{-1} were used for all intermediates[13]. The bath gas Ar was used in the present study, and ε = 78.88 cm^{-1} and σ = 3.47 Å were employed[29]. In this work, the RRKM/ME simulations were performed using the MESS kinetic code[30]. The pressure-dependent and high-pressure-limit (HPL) rate constants were fitted to a modified Arrhenius Eq. (3),

$$k(T) = AT^n \exp(-E_a/RT) \quad (3)$$

where, A, n, and E_a correspond to the pre-exponential factor, the temperature exponent, and the activation energy of the reaction, respectively. In addition, two-parameter fitting was adopted for

Table 1. List of the Arrhenius parameters for the rate constants of isomerization and β-scission reactions of UDMH radicals, as well as the H-abstraction reactions of the $HNN(CH_3)_2$ radical and subsequent decomposition reactions at HPL or 100 atm conditions.

No.	Reactions	P (atm)	*A*	*n*	E_a (cal/mol)
1	$HNN(CH_3)_2 = H_2NN(CH_3)CH_2$	HPL	1.2258E−15	8.1005	37,245
2	$HNN(CH_3)_2 = cis\text{-}HNNCH_3 + CH_3$	HPL	1.3900E+12	0.78176	41,951
3	$HNN(CH_3)_2 = trans\text{-}HNNCH_3 + CH_3$	HPL	2.1770E+12	0.72387	36,806
4	$H_2NN(CH_3)CH_2 = H_2NNCH_2 + CH_3$	HPL	8.4385E+12	0.43102	29,575
5	$H_2NN(CH_3)CH_2 = CH_2NCH_3 + NH_2$	HPL	1.6031E+13	0.18499	14,279
6	$HNN(CH_3)_2 + NO_2 = NN(CH_3)_2 + cis\text{-}HONO$	100	7.3949E+20	−2.7812	1,607.6
			4.2465E+04	1.8100	−4,564.2
7	$HNN(CH_3)_2 + NO_2 = CH_2NCH_3 + ON(NH)(OH)$	100	2.3499E+02	2.0956	22,579
8	$HNN(CH_3)_2 + NO_2 = NN(CH_3)_2 + trans\text{-}HONO$	100	1.0116E+45	−9.5853	39,906
			5.7045E+10	0.19569	20,318
9	$HNN(CH_3)_2 + NO_2 = CH_2NCH_3 + NN(OH)_2$	100	3.9191E+03	1.6501	21,623
10	$HNN(CH_3)_2 + NO = NN(CH_3)_2 + HNO$	100	1.7593E+03	2.2232	15,951
11	$HNN(CH_3)_2 + NO = HNN(CH_3)CH_2 + HNO$	100	5.1298E+03	2.1753	24,033
12	$HNN(CH_3)_2 + NO = NN(CH_3)_2 + NOH$	100	2.7881E+02	2.6552	41,967
13	$HNN(CH_3)_2 + NO = HNN(CH_3)CH_2 + NOH$	100	2.4904E−01	3.3194	46,582
14	$NN(CH_3)_2 = HNN(CH_3)CH_2$	HPL	3.7076E+10	0.99227	48,700
15	$NN(CH_3)_2 = N_2 + C_2H_6$	HPL	6.2976E+10	1.5546	36,030
16	$HNN(CH_3)CH_2 = HNNCH_2 + CH_3$	HPL	3.5255E+12	0.29155	53,875

reactions exhibiting non-Arrhenius behavior. The Arrhenius parameters of the relevant reactions of $HNN(CH_3)_2$ calculated in this work are provided in Table 1.

The influences of tunneling and hindered rotor treatments on the rate constants were comprehensively evaluated. As depicted in Supplementary Figs. S1–S4, the effect of tunneling on the calculated rate constants is minor at high temperatures, while the effect on R1 becomes significant at low temperatures. Moreover, the hindered rotor treatments also have little effect, except in the cases of R6 and R12. Additionally, the uncertainty analyses of the energy barrier and collisional parameter were performed on the calculated rate constants for the decomposition of UDMH radical. Supplementary Fig. S5 indicates that a variation of ± 1 kcal/mol in the energy barriers introduces only minor errors for reactions R1 to R4, particularly at high temperatures. In contrast, the error for R5 is relatively higher at 300 K. Generally, the uncertainties are more significant at lower temperatures than at higher ones. Regarding the collisional parameter, Supplementary Fig. S6 shows that the influence of σ on the rate constants is negligible. As depicted in Supplementary Fig. S7, additionally, a comparison of the rate constants with and without consideration of the vdW complexes revealed negligible effects for reactions R7, R8, R11, and R12, and differences for reactions R9 and R10 at low temperatures.

Results and discussion

Isomerization and β-scission reactions of $HNN(CH_3)_2$ radical

For the $HNN(CH_3)_2$ radical, the isomerization and β-scission reactions were investigated, with the PES results shown in Fig. 1. The H-migration isomerization reaction of $HNN(CH_3)_2$ (R1) has a relatively high energy barrier of 55.2 kcal/mol and the energy of the product $H_2NN(CH_3)CH_2$ radical is 12.0 kcal/mol higher than the reactant. This radical can undergo β-scission reactions with energy barriers of 36.2 kcal/mol and 41.3 kcal/mol, producing *cis*-$HNNCH_3$ (R2) and *trans*-$HNNCH_3$ (R3), respectively. This indicates that the β-N-C bond energies in $HNN(CH_3)_2$ are not uniform. Two β-scission channels were identified for the formed $H_2NN(CH_3)CH_2$: one corresponds to β-N-C bond dissociation, yielding H_2NNCH_2 and CH_3 (R4), whereas the other involves β-N-N bond dissociation, producing CH_2NCH_3 and NH_2 (R5). Their calculated energy barriers are 41.0 kcal/mol and 26.0 kcal/mol, respectively.

To illustrate the effects of increasing the number of CH_3 groups (relative to MMH) on the decomposition trends of UDMH radicals, a comparison was carried out between the energy barriers of isomerization and β-scission reactions in UDMH radicals and those of MMH radicals with similar configurational characteristics (as shown in Fig. 2c–e). As shown in Table 2, the energy barrier for the isomerization reaction *cis*-$HNN(H)CH_3 = H_2NN(H)CH_2$ is lower than that of R1 by 5.9 kcal/mol. For β-N-C scission reactions that form CH_3 radical from the $HNN(CH_3)_2$ radical (R2 and R3), however, the calculated energy barriers are approximately 1 kcal/mol higher than those of *trans*-$HNN(H)CH_3$ and *cis*-$HNN(H)CH_3$. In addition, the energy barrier for the β-N-N scission reaction of the $H_2NN(CH_3)CH_2$ radical (R5) is comparable to that of the $H_2NN(H)CH_2$ radical. These similarities suggest that the β-scission reactions of UDMH radicals exhibit chemical properties comparable to those of MMH radicals.

Figures 3 and 4 show the rate constants and branching ratios for the consumption pathways of $HNN(CH_3)_2$ and $H_2NN(CH_3)CH_2$ radicals, respectively. From Fig. 3a–c, it is noticeable that as the pressures increase, the rate constants of the reactions R1, R2, and R3 all represent increasing trends. By comparison, the H-migration isomerization reaction of $HNN(CH_3)_2$ radical (R1) exhibits a much lower rate constants than the other two β-scission reactions (R2 and R3), due to its much higher energy barrier. Similarly, consistent with the trend in transition energy barriers, Fig. 3d depicts that despite the branching ratio of R3 decreasing with temperature, it still contributes up to 75% of $HNN(CH_3)_2$ decomposition at a temperature of 2,500 K. In addition, the contribution of another β-scission reaction (R2) increases with temperature and reaches 25%, implying that $HNN(CH_3)_2$ radical is predominantly decomposed through β-scission reactions. As shown in Fig. 4a–c, the rate constants of R1-R (the reverse reaction of R1), R4, and R5 also increase as the pressure rises. Furthermore, the $H_2NN(CH_3)CH_2$ radical shows a higher rate constant and branching ratio (> 85%) for β-N-N scission reaction to produce CH_2NCH_3 and NH_2 (R5). This is attributed to its relatively low energy barrier.

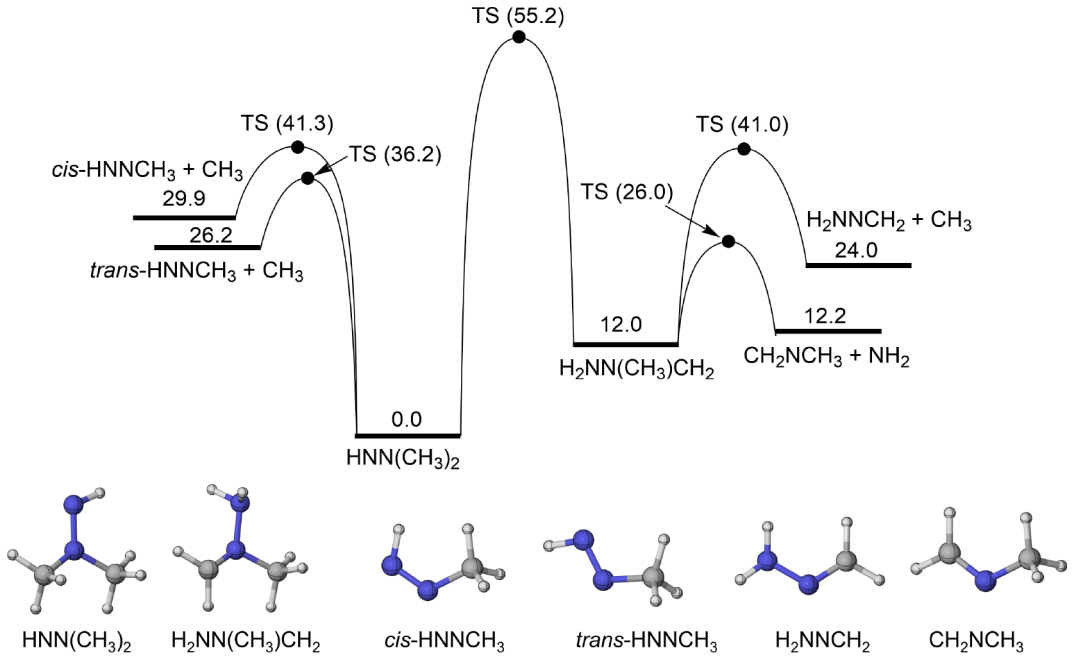

Fig. 1 PES for the isomerization and β-scission reactions of $HNN(CH_3)_2$ radical at CCSD(T)/CBS(D+T)//M06-2X/def2-TZVP level (unit: kcal/mol).

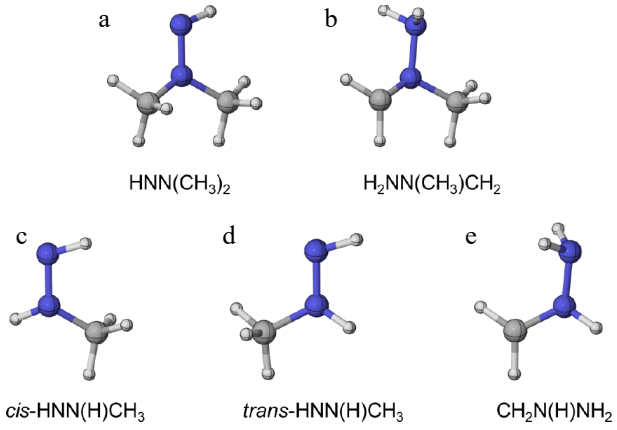

Fig. 2 The optimized molecular configurations of (a), (b) UDMH radicals at the M06-2X/def2-TZVP level of theory, and (c)–(e) MMH radicals at the CASPT2/aug-cc-pVTZ level of theory[31].

Sun et al.[31] comprehensively investigated the isomerization and β-scission reactions of MMH radicals (H_2NNCH_3, *trans*-$HNN(H)CH_3$, *cis*-$HNN(H)CH_3$, and $H_2NN(H)CH_2$). They found that *trans*-$HNN(H)CH_3$ and its cis isomer *cis*-$HNN(H)CH_3$ exhibited distinct behavior in their decomposition. In addition, the β-scission of the NH_2 group in $H_2NN(H)CH_2$ to form methyleneimine is the principal channel for this radical's decomposition. Here, to gain further insight into the differences between the UDMH and MMH radicals, the rate constants for their β-scission reactions with similar configurational characteristics were compared. As shown in Fig. 5a, b, the β-N-C scission reactions forming CH_3 radicals from $HNN(CH_3)_2$ and $HNN(H)CH_3$ exhibit comparable rate constants. Specifically, the differences between the rate constants for R2 and the reaction *trans*-$HNN(H)CH_3$ = *cis*-HNNH + CH_3[31] are within a factor of two at temperatures above 800 K. Moreover, R3 and its counterpart reaction, *cis*-$HNN(H)CH_3$ = *trans*-HNNH + CH_3[31], show an even smaller difference in rate constants. This demonstrates that methyl substitution on the central nitrogen atom of the UDMH radical has a subtle influence on the kinetics of β-N-C scission reactions, suggesting that an analogous strategy may be applicable when developing kinetic models for UDMH combustion.

Table 2. Comparison of the energy barrier for the isomerization and β-scission reactions of UDMH radicals with those of MMH radicals with similar configurational characteristics.

Reactions	Energy barrier (kcal/mol)	Ref.
trans-$HNN(H)CH_3$ = $H_2NN(H)CH_2$	49.3 (52.98)	This work ([31]*a*)
$HNN(CH_3)_2$ = $H_2NN(CH_3)CH_2$ (R1)	55.2	This work
trans-$HNN(H)CH_3$ = *cis*-HNNH + CH_3	42.2 (39.84)	This work ([31]*a*)
$HNN(CH_3)_2$ = *cis*-$HNNCH_3$ + CH_3 (R2)	41.3	This work
cis-$HNN(H)CH_3$ = *trans*-HNNH + CH_3	37.2 (35.19)	This work ([31]*a*)
$HNN(CH_3)_2$ = *trans*-$HNNCH_3$ + CH_3 (R3)	36.2	This work
$H_2NN(H)CH_2$ = CH_2NH + NH_2	13.5 (13.75)	This work ([31]*b*)
$H_2NN(CH_3)CH_2$ = CH_2NCH_3 + NH_2 (R5)	14.0	This work

[a] Results were obtained at the theory level of QCISD(T)/cc-pV∞Z//B3LYP/6-311++G(d,p); [b] Results were obtained at the theory level of QCISD(T)/cc-pV∞Z//CASPT2/aug-cc-pVTZ.

For β-N-N scission reactions forming NH_2 radicals (Fig. 5c), the rate constants of R5 and $H_2NN(H)CH_2$ = CH_2NH + NH_2[31] differ by approximately a factor of two within the temperature range of 800–2,500 K. However, this discrepancy increases significantly as the temperature decreases, reaching a factor of 63 at 300 K – a behavior distinct from that of β-N-C scission. This difference may arise from variations in the selected theoretical levels or inherent molecular properties. In summary, under the high-temperature conditions relevant to combustion, the kinetic properties of β-scission reactions in the UDMH radical are relatively similar to those of the MMH radical.

Addition-dissociation reactions of $HNN(CH_3)_2$ radical

NO_2 attacking

Considering the vital role of second H-abstraction reactions in the MMH/N_2O_4 combustion[13], the H-abstraction reactions of $HNN(CH_3)_2$ with NO_2 and NO were investigated in this work. As depicted in Fig. 6a–c, the reaction of $HNN(CH_3)_2$ with NO_2 yields

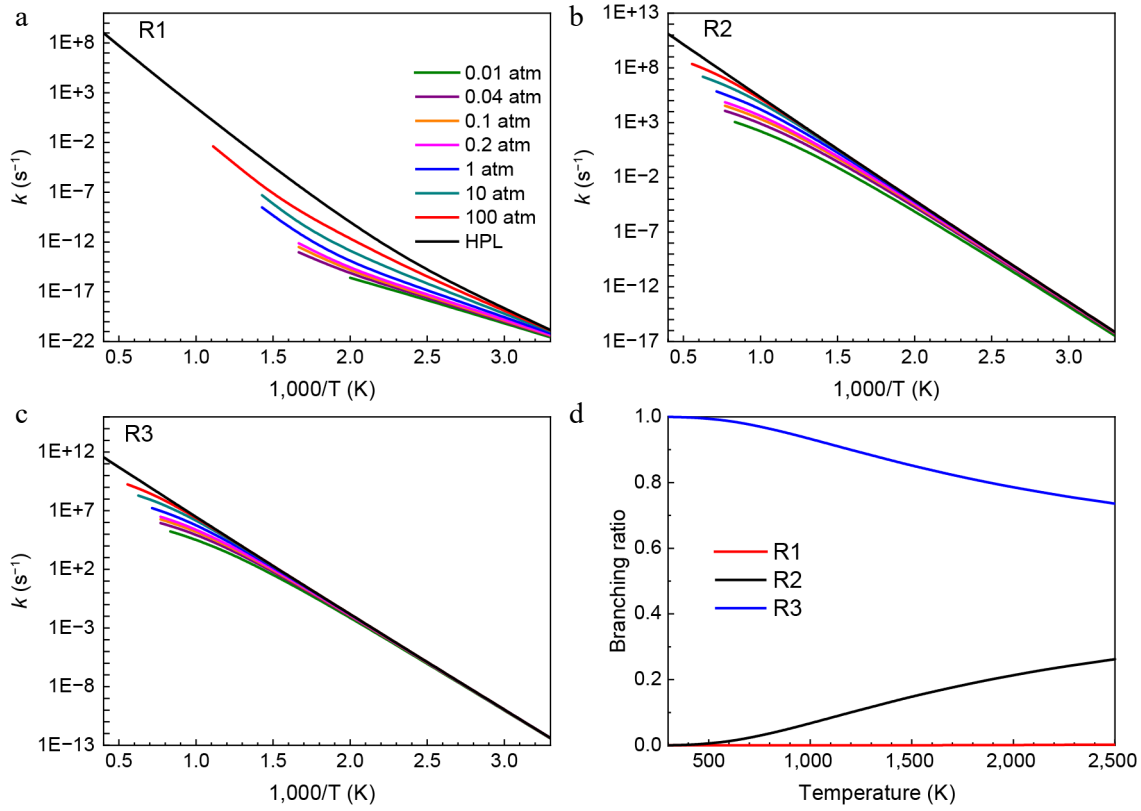

Fig. 3 Pressure-dependent rate constants for (a) R1, (b) R2, and (c) R3. (d) Branching ratios of all consumption reactions of $HNN(CH_3)_2$ radical at HPL.

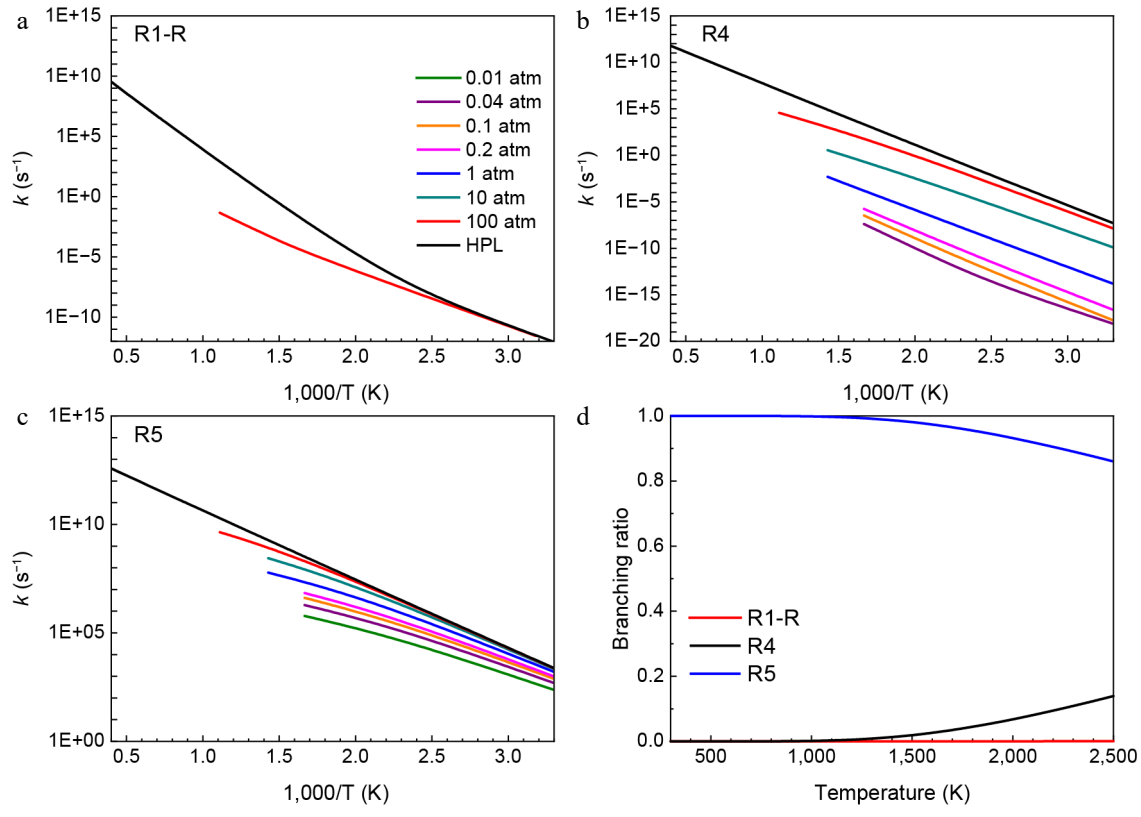

Fig. 4 Pressure-dependent rate constants for (a) R1-R, (b) R4, and (c) R5. (d) Branching ratios of all consumption reactions of $H_2NN(CH_3)CH_2$ radical at HPL.

three stable configurations, i.e., *cis*-ONON(H)N$(CH_3)_2$, *trans*-ONON(H)N$(CH_3)_2$, and $O_2NN(H)N(CH_3)_2$. Table 3 shows that the formation of *cis*-ONON(H)N$(CH_3)_2$ and *trans*-ONON(H)N$(CH_3)_2$ releases 17.2 and 13.5 kcal/mol, respectively. In contrast, the analogous reaction $NHN(H)CH_3 + NO_2 =$ *trans*-ONON(H)N(H)CH_3 release 17.99 kcal/mol[12], which is higher than that of *trans*-ONON(H)N$(CH_3)_2$, despite their

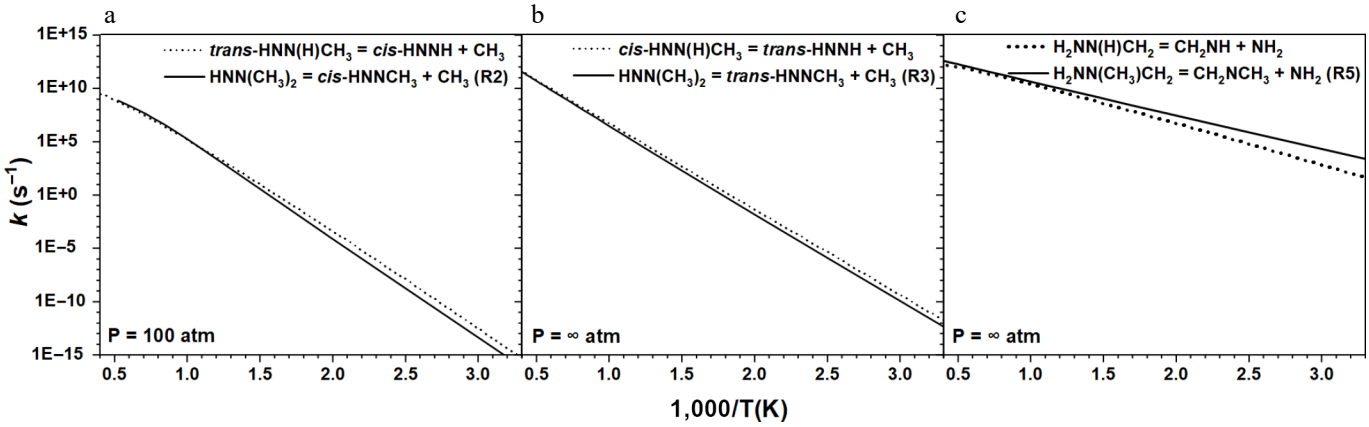

Fig. 5 Comparison of the rate constants for the β-scission reactions of (a), (b) $HNN(CH_3)_2$, and (c) $H_2NN(CH_3)CH_2$ radicals with those of MMH radicals with similar configurational characteristics[31].

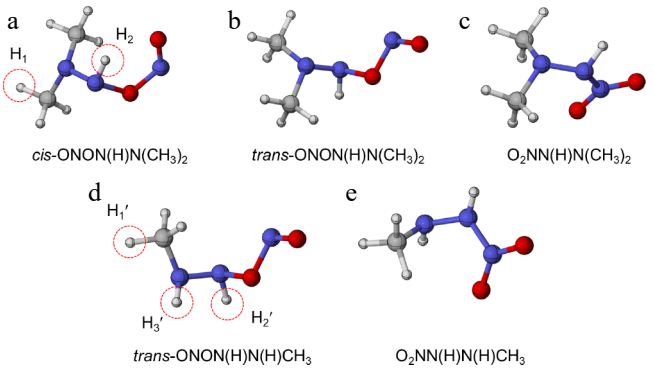

Fig. 6 The optimized molecular configurations of (a)–(c) $HNN(CH_3)_2$ + NO_2 at the M06-2X/def2-TZVP level of theory, and (d) $NHN(H)CH_3$ + NO_2 at the ωB97X-D/6-311++G(d,p) level of theory[12].

Table 3. Relative energies of $HNN(CH_3)_2$ + NO_2 at the CCSD(T)/CBS(D+T)//M062X/def2-TZVP level of theory and $NHNHCH_3$ + NO_2 at the RHF-UCCSD(T)-F12//ωB97X-D/6-311++G(d,p) level of theory[12].

Reactions	Relative energy (kcal/mol)	Ref.
$HNN(CH_3)_2 + NO_2 = cis\text{-}ONON(H)N(CH_3)_2$	−17.2	This work
$HNN(CH_3)_2 + NO_2 = trans\text{-}ONON(H)N(CH_3)_2$	−13.5	This work
$HNN(CH_3)_2 + NO_2 = O_2NN(H)N(CH_3)_2$	−31.7	This work
$NHN(H)CH_3 + NO_2 = trans\text{-}ONON(H)N(H)CH_3$	−17.99	[12]
$NHN(H)CH_3 + NO_2 = O_2NN(H)N(H)CH_3$	−33.84	[12]

similar configurations. For N-N bond formation reactions, the energy released from $HNN(CH_3)_2$ + NO_2 (31.7 kcal/mol) is slightly lower than that from $NHN(H)CH_3$ + NO_2 (33.84 kcal/mol)[12]. However, no stable transition state was found for the subsequent reactions of *trans*-$ONON(H)N(CH_3)_2$, differing from the reaction characteristics observed for $NHN(H)CH_3$ + NO_2[12,13]. Consequently, the following PES analysis and rate constant calculations focus exclusively on the subsequent reactions of *cis*-$ONON(H)N(CH_3)_2$ and $O_2NN(H)N(CH_3)_2$.

In the $HNN(H)CH_3$ radical, there are three types of hydrogen atoms: those at the primary carbon sites (H_1′), and those bonded to nitrogen (H_2′ and H_3′). In contrast, the $HNN(CH_3)_2$ radical lacks H_3′ due to substitution of the H atom by a CH_3 group, retaining only H_1′ and H_2′. Bai et al.[13] and Kanno et al.[12] found that reactions of $HNN(H)CH_3$ with NO_2 primarily produce $HNNCH_3$ via abstraction of the H atom at H_3′. However, the formation reaction pathways of the related $NN(H)CH_3$ radical remain unexplored. In $HNN(CH_3)_2$, this reaction behavior is altered due to the absence of H_3′.

As depicted in Fig. 7, *cis*-$ONON(H)N(CH_3)_2$ undergoes a reaction with a low energy barrier of 0.4 kcal/mol, leading to the formation of a product complex (PC) via the abstraction of the H_2′ atom. This product complex ultimately dissociates to generate $NN(CH_3)_2$ and *cis*-HONO (R6). In contrast, the decomposition of $O_2NN(H)N(CH_3)_2$ proceeds via more complex reaction channels. The first pathway requires a relatively high energy barrier of 49.7 kcal/mol to pass through a transition state involving intramolecular H-immigration from the primary carbon site to the O atom of the NO_2 molecule, subsequently generating CH_2NCH_3 and ON(NH)(OH) (R7). In addition, $HO_2NNN(CH_3)_2$ can be formed from $O_2NN(H)N(CH_3)_2$ via a relatively low energy barrier of 36.4 kcal/mol. Subsequently, this product decomposes into $NN(CH_3)_2$ and *trans*-HONO via a transition state with an energy barrier of 20.5 kcal/mol. Additionally, $HO_2NNN(CH_3)_2$ undergoes a multi-well reaction pathway, ultimately leading to the formation of CH_2NCH_3 and $NN(OH)_2$.

Figure 8 shows the rate constants of addition-dissociation reactions of the $HNN(CH_3)_2$ radical with NO_2 at different pressure conditions. It is evident that the rate constants of reactions R6–R9 decrease with increasing pressure. Particularly, when the temperature is low (300 K), the rate constants of R8 at 0.01 atm and 100 atm differ by as much as six orders of magnitude. In addition, the rate constant of R6 exceeds 1×10^{11} cm^3 mol^{-1} s^{-1}, which is significantly higher than those of the other reactions due to a negative energy barrier. Based on the PES and rate constants, it can be inferred that $NN(CH_3)_2$ is favorably formed in the addition-dissociation reaction of the $HNN(CH_3)_2$ radical with NO_2. Vaghjiani et al.[32] calculated the potential energy surface of the N_2H_3 + NO_2 system, which is more complex compared to the reaction involving $HNN(CH_3)_2$ and NO_2. For the N_2H_3 + NO_2 system, at low temperatures, the channel leading to the formation of *trans*-N_2H_2 and *trans*-HONO is dominant. In contrast, the channel which produces $NN(CH_3)_2$ + *cis*-HONO has the most important contribution within the entire temperature range investigated in this work.

NO attacking

Figure 9 presents the PESs for the addition-dissociation reactions of the $HNN(CH_3)_2$ radical with the NO molecule. Four reaction pathways are identified based on the resulting products (HNO and NOH). Three intermediates, i.e., $ONN(H)N(CH_3)_2$-1, $ONN(H)N(CH_3)_2$-2, and $ONN(H)N(CH_3)_2$-3, are formed when $HNN(CH_3)_2$ reacts with NO, releasing 24.7, 22.8, and 23.7 kcal/mol of energy, respectively. For the formation of HNO, there are two main reaction channels. In the first pathway, $ONN(H)N(CH_3)_2$-1 overcomes an energy barrier of 41.1 kcal/mol, then the formed product complex decomposes into

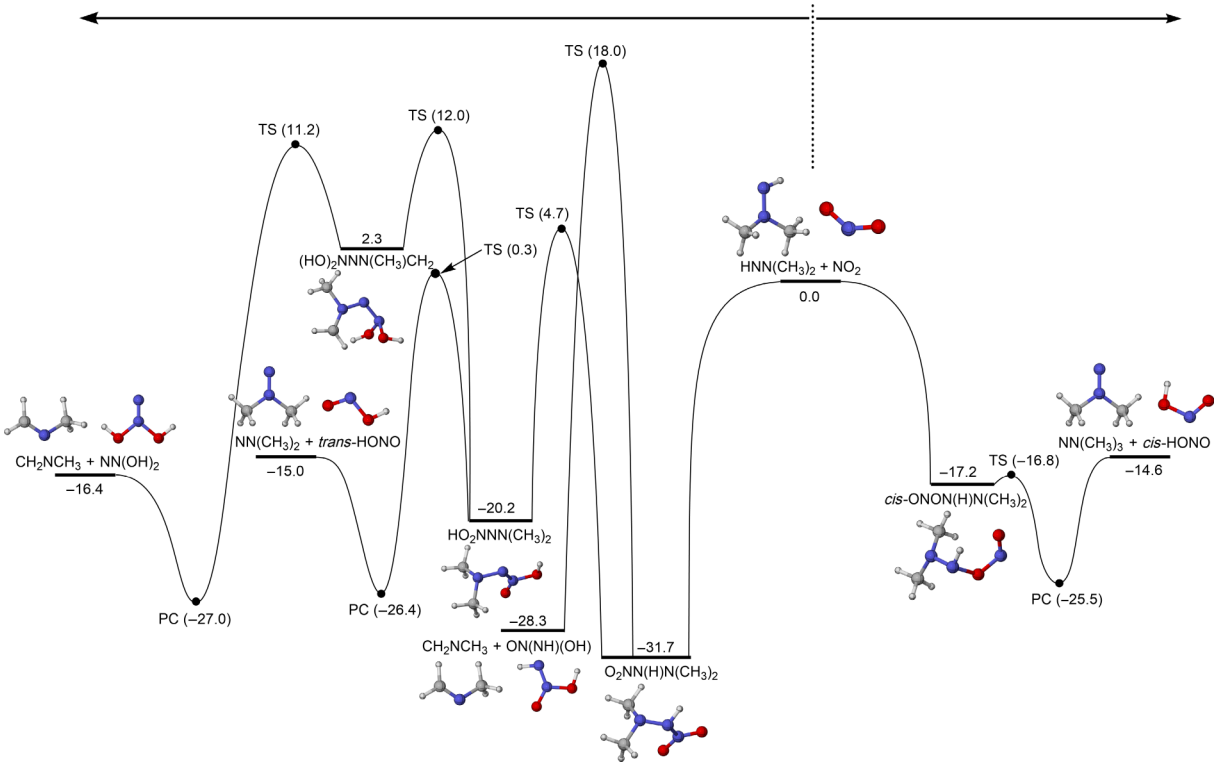

Fig. 7 PESs for the addition-dissociation reactions of $HNN(CH_3)_2$ with NO_2 at CCSD(T)/CBS(D+T)//M06-2X/def2-TZVP level of theory (unit: kcal/mol).

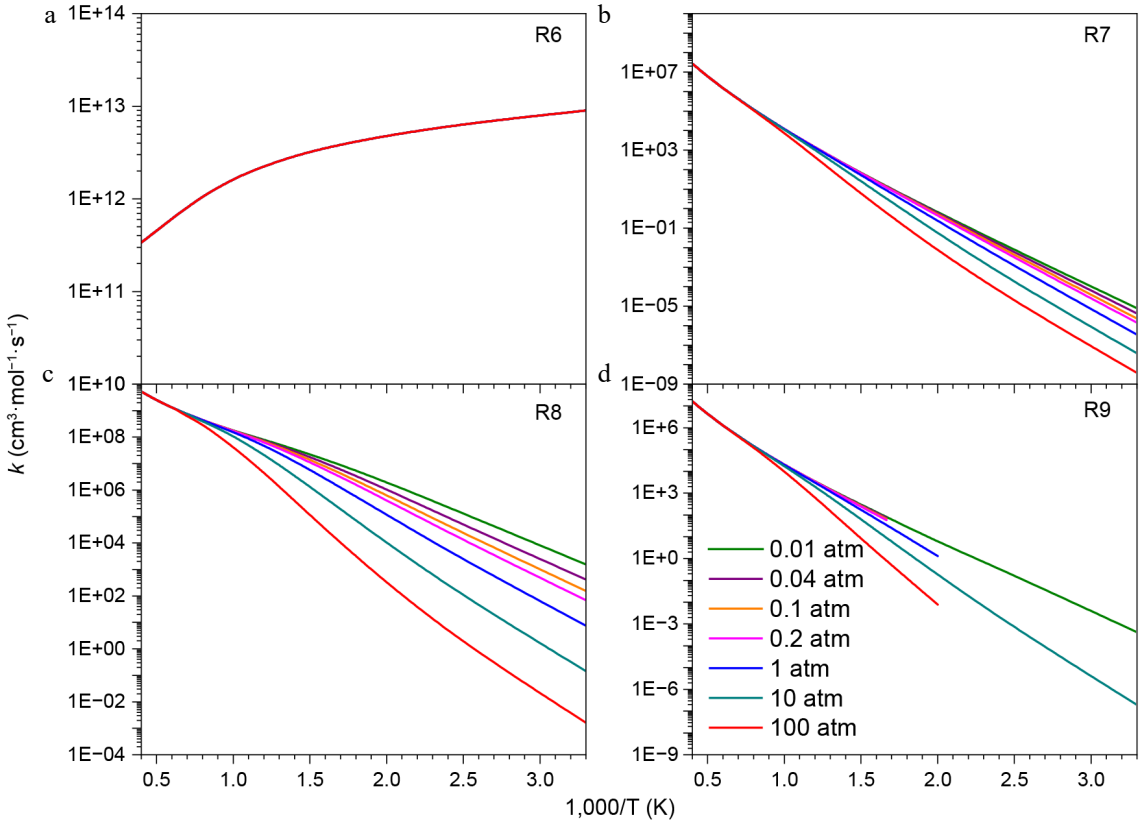

Fig. 8 Pressure-dependent rate constants for the addition-dissociation reactions of $HNN(CH_3)_2$ radical with NO_2.

$NN(CH_3)_2$ and HNO (R10). The second pathway requires a relatively higher energy barrier of 45.8 kcal/mol and leads to the transformation of $ONN(H)N(CH_3)_2$-1 into $HNN(CH_3)CH_2$ and HNO (R11). For NOH formation, $ONN(H)N(CH_3)_2$-3 proceeds through a three-membered transition state with an energy barrier of 66.7 kcal/mol to form $NN(CH_3)_2$ and NOH (R12). The entire process requires a total energy

input of 82.0 kcal/mol, which is higher than that of the other three reactions. When the O atom of NO attacks the H atom at the primary carbon (R14) directly, the energy barrier of the H-abstraction reaction is 48.6 kcal/mol, and the overall energy required to form $HNN(CH_3)CH_2$ and NOH (R13) is 56.8 kcal/mol.

Figure 10 shows the rate constants for the addition-dissociation reactions of $HNN(CH_3)_2$ with the NO molecule based on the PES results. It is evident that reactions R12 and R13 exhibit lower rate constants due to their higher energy barriers. R10 has the lowest barrier among the four reactions, demonstrating the highest reaction rate. As the reaction temperature increases, the differences in rate constants among the four reactions gradually decrease. As depicted in Fig. 10b, the branching ratio of R10 decreases with increasing temperature and reaches 70% at 2,500 K. Another HNO formation reaction (R11) plays a secondary role in the addition-dissociation reactions of $HNN(CH_3)_2$ with NO. In addition, the NOH formation reactions make smaller contributions. According to the calculated results for the addition-dissociation reactions of $HNN(CH_3)_2$ with NO_2 and NO, it can be concluded that $NN(CH_3)_2$ is readily formed.

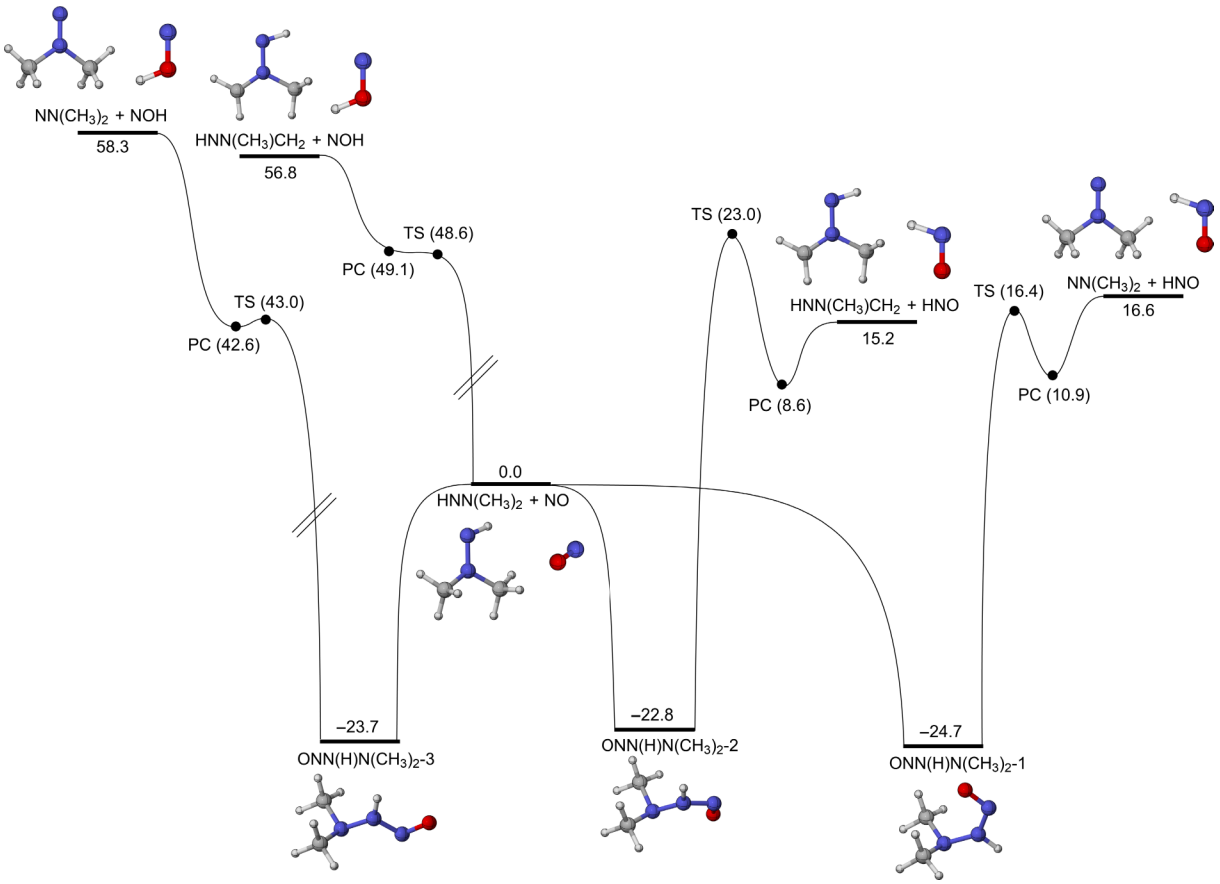

Fig. 9 PESs for the addition-dissociation reactions of $HNN(CH_3)_2$ with NO at CCSD(T)/CBS(D+T)//M06-2X/def2-TZVP level of theory (unit: kcal/mol).

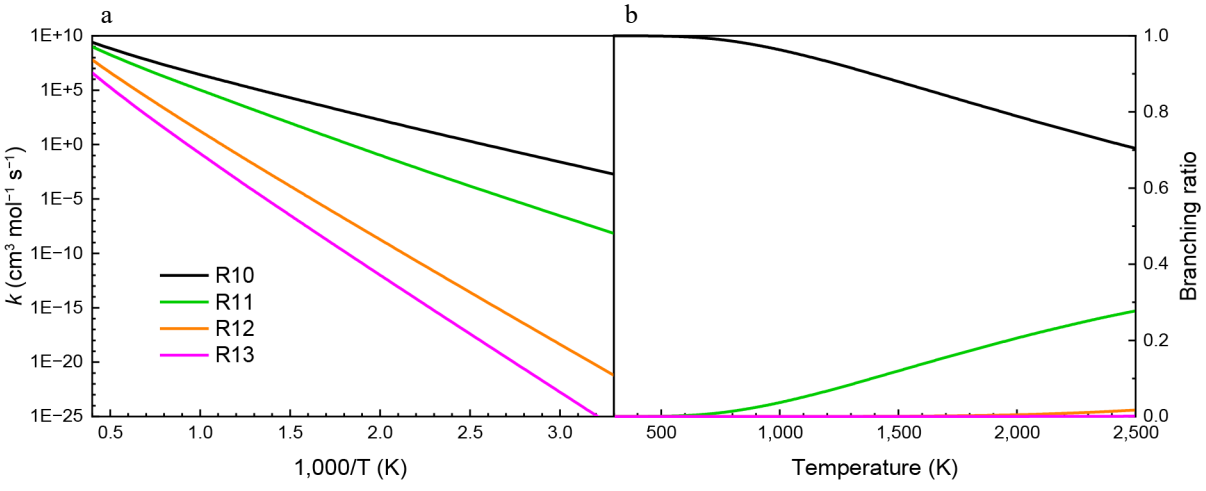

Fig. 10 (a) Rate constants, and (b) branching ratios for the addition-dissociation reactions of $HNN(CH_3)_2$ with NO at HPL.

Subsequent decomposition reactions of $NN(CH_3)_2$

Considering that $NN(CH_3)_2$ is easy to form, its subsequent consumption reactions were studied. As shown in Fig. 11, the H-migration isomerization reaction (R14) of $NN(CH_3)_2$ to generate the $HNN(CH_3)CH_2$ radical has an energy barrier of 48.7 kcal/mol. The calculations also indicate that $NN(CH_3)_2$ can dissociate to produce N_2 and C_2H_6 (R15), with an energy barrier of 34.9 kcal/mol and releasing 83.4 kcal/mol of energy. This barrier is 13.8 kcal/mol lower than that of the H-migration isomerization reaction, making R15 the more favorable pathway. In addition, the β-N-C scission of the $HNN(CH_3)CH_2$ radical to form $HNNCH_2$ and CH_3 (R16) has a higher energy barrier of 53.4 kcal/mol. Rate constant calculations under varying pressures, as presented in Fig. 12, further demonstrate that R15 has a higher rate constant, as a result of its relatively lower energy barrier. Furthermore, the rate constants of R14 and its reverse reaction (R14-R) exhibit strong pressure dependence, particularly at high temperatures, whereas the pressure effects on R15 and R16 are comparatively weaker, especially at lower temperatures.

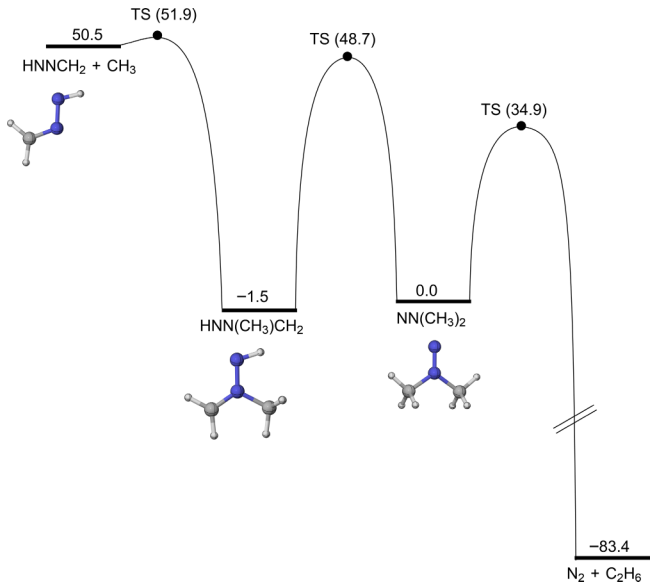

Fig. 11 PESs for the isomerizartion and β-scission reactions of $NN(CH_3)_2$ at CCSD(T)/CBS(D+T)//M06-2X/def2-TZVP level of theory (unit: kcal/mol).

Conclusions

In this work, the decomposition reactions of $HNN(CH_3)_2$ radical, including the isomerization, β-scission, and H-abstraction reactions, were theoretically investigated at the CCSD(T)/CBS(D+T)//M06-2X/def2-TZVP level of theory. Pressure-dependent rate constants of isomerization and β-scission reactions of $HNN(CH_3)_2$ were determined by solving the RRKM/ME equations. Additionally, the subsequent decomposition reactions of $NN(CH_3)_2$ were also studied. Comparative analyses with MMH radicals were conducted to elucidate the effects of CH_3 group substitution on the kinetic characteristics of UDMH radical decomposition. The key findings can be summarized as follows:

(1) For the isomerization and β-scission reactions of UDMH radicals, $HNN(CH_3)_2$ undergoes β-scission (forming $HNNCH_3$) more readily than H-migration isomerization. For the $H_2NN(CH_3)CH_2$ radical, the β-N-N scission reaction that produces CH_2NCH_3 and NH_2 is

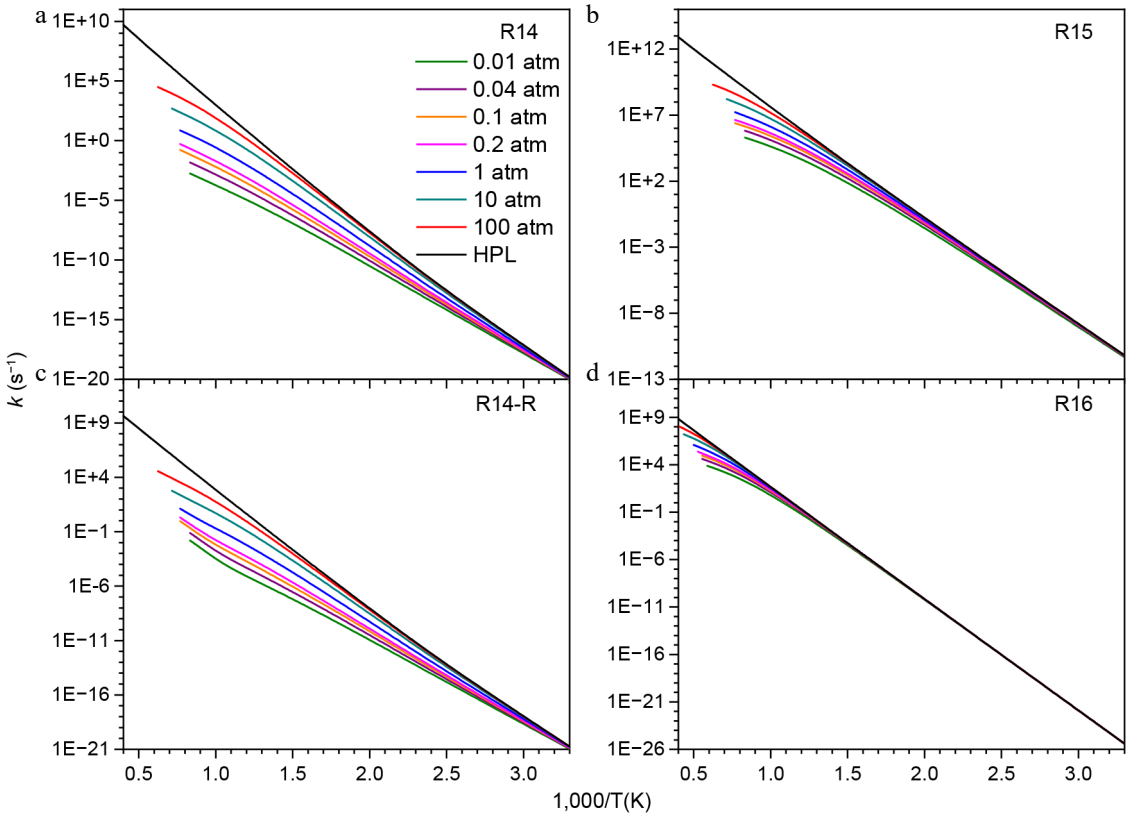

Fig. 12 Pressure-dependent rate constants for the consumption reactions of $NN(CH_3)_2$.

characterized by a relatively lower energy barrier and a higher rate constant.

(2) For the H-abstraction reactions of $HNN(CH_3)_2$ by NO_2, the pathway forming $NN(CH_3)_2$ and *cis*-HONO via the decomposition of *cis*-$ONON(H)N(CH_3)_2$ has the lowest energy barrier and the highest rate constants. Similarly, H-abstraction by NO also readily yields $NN(CH_3)_2$. Subsequently, $NN(CH_3)_2$ dissociates into N_2 and C_2H_6 through a pathway with a relatively low energy barrier.

(3) Based on the comparison, the kinetic properties of β-scission reactions in UDMH radicals are similar to those in MMH radicals. However, the H-abstraction of $HNN(CH_3)_2$ by NO_2 differs significantly from that of the MMH radical ($HNN(H)CH_3$). $HNN(CH_3)_2$ primarily undergoes H-abstraction at the terminal nitrogen site to form $NN(CH_3)_2$, whereas $HNN(H)CH_3$ favors H-abstraction from the central nitrogen atom. The obtained fundamental kinetic parameters provide critical inputs for refining detailed chemical kinetic models of hydrazine-based propellant combustion.

Author contributions

The authors confirm contributions to the paper as follows: study conception and design: Li Y; investigation: Zhang Y, Fang Q, Fang J; formal analysis: Zhang Y, Fang Q; data analysis: Li W; draft manuscript preparation: Li W, Zhang Y, Fang Q; manuscript revision: Li W, Fang Q, Li Y. All authors reviewed the results and approved the final version of the manuscript.

Data availability

The theoretically calculated and analytical data obtained in this work are included in this published article.

Acknowledgments

This research received no specific grant from any funding agency, commercial or not-for-profit sectors.

Conflict of interest

The authors declare that they have no conflict of interest.

Supplementary information accompanies this paper online at (https://doi.org/10.48130/prkm-0025-0028)

Dates

Received 8 August 2025; Revised 4 November 2025; Accepted 12 November 2025; Published online 9 January 2026

References

[1] Milyushkin AL, Karnaeva AE. 2023. Unsymmetrical dimethylhydrazine transformation products: a review. *Science of The Total Environment* 891:164367

[2] Zheng M, Zhang X. 2025. Insights into the NO removal mechanism by hydrazine. *Progress in Reaction Kinetics and Mechanism* 50:e003

[3] Liu D, Zhang L, Zhang P. 2025. Ab inito chemical kinetics modeling of liquid-phase reactions of monomethylhydrazine and nitrogen tetroxide. *The Journal of Physical Chemistry A* 129:4148−4161

[4] Cheng Y, Mao Q, Shi B, Hou X. 2025. A detailed kinetic model for the pyrolysis and oxidation of monomethylhydrazine. *Combustion and Flame* 279:114328

[5] Diévart P, Catoire L. 2020. Contributions of experimental data obtained in concentrated mixtures to kinetic studies: application to monomethylhydrazine pyrolysis. *The Journal of Physical Chemistry A* 124:6214−6236

[6] Hu HB, Chen HY, Yan Y, Zhang F, Yin JH, et al. 2021. Investigation of chemical kinetic model for hypergolic propellant of monomethylhydrazine and nitrogen tetroxide. *Journal of Energy Resources Technology* 143:062304

[7] Sun H, Law CK. 2007. Thermochemical and kinetic analysis of the thermal decomposition of monomethylhydrazine: an elementary reaction mechanism. *The Journal of Physical Chemistry A* 111:3748−3760

[8] Sun H, Vaghjiani GL, Law CK. 2020. *Ab Initio* kinetics of methylamine radical thermal decomposition and H-abstraction from monomethylhydrazine by H-atom. *The Journal of Physical Chemistry A* 124:3747−3753

[9] Tang Y, Lu C, Han Z, Zhai F, Fu Z. 2019. Theoretical investigations on mechanisms and kinetics of OH + $(CH_3)_2NNH_2$ reaction in the atmosphere. *Theoretical Chemistry Accounts* 138:45

[10] Wang L, Zhao Y, Wen J, Zhang J. 2012. Mechanisms and kinetics of hydrogen abstraction of methylhydrazine and deuterated methylhydrazine with H/D atoms. *Theoretical Chemistry Accounts* 132:1321

[11] Kanno N, Kito T. 2020. Theoretical study on the hydrogen abstraction reactions from hydrazine derivatives by H atom. *International Journal of Chemical Kinetics* 52:548−555

[12] Kanno N, Tani H, Daimon Y, Terashima H, Yoshikawa N, et al. 2015. Computational study of the rate coefficients for the reactions of NO_2 with CH_3NHNH, CH_3NNH_2, and CH_2NHNH_2. *The Journal of Physical Chemistry A* 119:7659−7667

[13] Bai J, Liu D, Zhang L, Zhang P. 2024. Theoretical study of the second- and third-H-abstraction reactions of monomethylhydrazine and nitrogen dioxide and its application to hypergolic ignition modeling. *Combustion and Flame* 268:113617

[14] Zhang Y, Fang Q, Han S, Fang J, Li W. 2025. Ab initio kinetic study on the unimolecular decomposition and H-abstraction reactions of unsym-dimethylhydrazine. *Progress in Reaction Kinetics and Mechanism* submitted

[15] Zhao Y, Truhlar DG. 2008. The M06 suite of density functionals for main group thermochemistry, thermochemical kinetics, noncovalent interactions, excited states, and transition elements: two new functionals and systematic testing of four M06-class functionals and 12 other functionals. *Theoretical Chemistry Accounts* 120:215−241

[16] Schäfer A, Huber C, Ahlrichs R. 1994. Fully optimized contracted Gaussian basis sets of triple zeta valence quality for atoms Li to Kr. *The Journal of Chemical Physics* 100:5829−5835

[17] Bao JL, Zheng J, Alecu IM, Lynch BJ, Zhao Y, et al. n.d. *Database of Frequency Scale Factors for Electronic Model Chemistries (Version 3 Beta 2)*. https://comp.chem.umn.edu/freqscale/version3b2.htm

[18] Martin JML. 1996. Ab initio total atomization energies of small molecules – towards the basis set limit. *Chemical Physics Letters* 259:669−678

[19] Lee TJ, Taylor PR. 1989. A diagnostic for determining the quality of single-reference electron correlation methods. *International Journal of Quantum Chemistry* 36:199−207

[20] Frisch MJ, Schlegel HB, Scuseria GE, Robb MA, Cheeseman JR, et al. 2013. *Gaussian 09, Revision D. 01*. Wallingford CT: Gaussian, Inc

[21] Andersson K, Malmqvist PÅ, Roos BO. 1992. Second-order perturbation theory with a complete active space self-consistent field reference function. *The Journal of Chemical Physics* 96:1218−1226

[22] Bai J, Liu D, Zhang L, Zhou L, Zhang P. 2025. Towards hypergolic ignition modeling of monomethylhydrazine and nitrogen dioxide: Ab initio chemical kinetics of $CH_3NH/CH_2NH_2/CH_2NH$ and nitrogen dioxide. *Combustion and Flame* 275:114034

[23] Halkier A, Klopper W, Helgaker T, Jørgensen P, Taylor PR. 1999. Basis set convergence of the interaction energy of hydrogen-bonded complexes. *The Journal of Chemical Physics* 111:9157−9167

[24] Klippenstein SJ, Cline JI. 1995. Classical phase space theory for product state distributions with application to the *v*–*j* vector correlation. *The Journal of Chemical Physics* 103:5451−5460

[25] Cavallotti C, Pelucchi M, Georgievskii Y, Klippenstein SJ. 2019. EStokTP: electronic structure to temperature- and pressure-dependent rate constants – a code for automatically predicting the thermal kinetics of reactions. *Journal of Chemical Theory and Computation* 15:1122–1145

[26] Miller JA, Klippenstein SJ. 2006. Master equation methods in gas phase chemical kinetics. *The Journal of Physical Chemistry A* 110:10528–10544

[27] East ALL, Radom L. 1997. *Ab initio* statistical thermodynamical models for the computation of third-law entropies. *The Journal of Chemical Physics* 106:6655–6674

[28] Eckart C. 1930. The penetration of a potential barrier by electrons. *Physical Review* 35:1303–1309

[29] Mourits FM, Rummens FHA. 1977. A critical evaluation of Lennard–Jones and Stockmayer potential parameters and of some correlation methods. *Canadian Journal of Chemistry* 55:3007–3020

[30] Georgievskii Y, Miller JA, Burke MP, Klippenstein SJ. 2013. Reformulation and solution of the master equation for multiple-well chemical reactions. *The Journal of Physical Chemistry A* 117:12146–12154

[31] Sun H, Zhang P, Law CK. 2012. Ab initio kinetics for thermal decomposition of $CH_3N{\bullet}NH_2$, *cis*-$CH_3NHN{\bullet}H$, *trans*-$CH_3NHN{\bullet}H$, and $C{\bullet}H_2NNH_2$ Radicals. *The Journal of Physical Chemistry A* 116:8419–8430

[32] Vaghjiani GL, Sun H, Chambreau SD. 2020. Experimental and theoretical investigations of the radical–radical reaction: $N_2H_3 + NO_2$. *The Journal of Physical Chemistry A* 124:10434–10446